



# Synthesis, characterization and evaluation of iron oxides and niobium in the removal of dyes in Fenton type reactions and photocatalysis

Síntese, caracterização e avaliação de óxidos de ferro e nióbio na remoção de corantes em reações do tipo Fenton e fotocatalise

J. S. Ferreira<sup>1</sup>, T. S. Santos<sup>2</sup>, M. O. G. Souza<sup>2</sup>, A. R. Martins<sup>1\*</sup>

<sup>1</sup>Instituto Federal da Bahia – Campus Porto Seguro, Fontana 1, 45810-000, Porto Seguro-BA, Brasil

<sup>2</sup>Universidade do Estado da Bahia, Departamento de Ciências Exatas e da Terra, 41195-001, Salvador-BA, Brasil

\* andremartins@ifba.edu.br

(Recebido em 26 de agosto de 2020; aceito em 08 de dezembro de 2020)

In this work, catalysts based on niobium oxide modified with iron oxide were developed for the photocatalytic treatment of effluents contaminated with dyes. The catalysts were prepared, in different proportions of niobium and iron, using niobium ammonium oxalate salts, iron nitrate and ammonium acetate and calcination at 400 °C. The solids were characterized by X-ray diffraction, infrared spectroscopy with Fourier transform, measured at zero point charge and evaluated in adsorption, Fenton reaction type advanced oxidation and methylene blue heterogeneous photocatalysis. It was observed that the increase in niobium concentration increased the values of point of zero charge and decreased the reaction system final pH. The solid with Fe/Nb2 ratio showed the best performance as an adsorbent and in oxidation reaction, followed by the one with Fe / Nb1.5 ratio. The solids showed practically the same result (1.8 eV), in addition, the presence of iron niobite (Fe/Nb1) favored the photocatalytic system.

Keywords: Fenton, photocatalysis, niobium oxide

Neste trabalho foram desenvolvidos catalisadores com base em óxido de nióbio modificado com óxido de ferro, para o tratamento fotocatalítico de efluentes contaminados com corantes. Os catalisadores foram preparados, em diferentes proporções de nióbio e ferro, utilizando-se sais oxalato amoniacal de nióbio, nitrato de ferro e acetato de amônio, e calcinação a 400 °C. Os sólidos foram caracterizados por difração de raios X, espectroscopia na região do infravermelho com transformada de Fourier, medida do ponto de carga zero e avaliadas na adsorção, oxidação avançada do tipo reação Fenton e fotocatalise heterogênea do azul de metileno. Foi observado que o aumento da concentração de nióbio elevou os valores de ponto de carga zero e diminuiu o pH final do sistema reacional. O sólido com razão Fe/Nb 2 apresentou o melhor desempenho como adsorvente, seguido do sólido com razão Fe/Nb 1.5. Os sólidos apresentaram praticamente o mesmo resultado (1,8 eV), sendo que a presença de niobato de ferro (Fe/Nb1) favoreceu o sistema fotocatalítico.

Palavras chave: Fenton, fotocatalise, óxido de nióbio

## 1. INTRODUCTION

Industrial effluents, rich in toxic organic compounds, have generated high pollution to the environment. In addition, the increase in water consumption reinforces the importance of efficient treatments for the degradation of various organic pollutants which are characterized by resistance to conventional treatments and long residence time in the environment. This promotes a constant search for physical-chemical processes that can remove these contaminants efficiently and at a low cost [1].

A variety of processes have been proposed, some of which are widely used industrially, such as the flotation / sedimentation system and activated carbon adsorption [1]. These ones have the disadvantage of not being destructive [2, 3]. The treatment by biological processes, on the other hand, decomposes the pollutant; however, it is limited, not being efficient in the degradation of organochlorines and phenols, for example [4].

The so-called Advanced Oxidative Processes (AOP) have gained prominence as an alternative for the effluents treatment contaminated by toxic organic compounds. These processes are based

on the formation of highly oxidizing species. In this sense, the formation of hydroxyl-type radicals is desirable. Such contaminant elimination processes stand out for their efficiency since they are not selective, being able to eliminate a wide variety of organic compounds, transforming them into carbon dioxide, water and inorganic anions [5].

Among the AOPs, the following can be highlighted: heterogeneous photocatalysis, processes based on Fenton and photo-Fenton reactions and processes based on ozone reaction. Photocatalysis stands out for using fewer reagents and being efficient. Heterogeneous photocatalysis uses semiconductors which are activated by ultraviolet radiation in order to promote valence band electrons for conduction band [6], thus generating a positive gap in the first one. Titanium oxide is the main semiconductor, but other semiconductors, such as zinc oxide and iron oxides, perform well [5].

In the case of iron oxide, it is worth mentioning the fact that phases, such as goethite and hematite, which have low activity in other AOP systems, such as Fenton, are very active in photocatalysis [1, 7].

A material that has also excelled in photocatalysis is niobium oxide. It has semiconductor properties, redox capability and is active in hydrogen peroxide decomposition reactions [8]. In addition, Brazil is the world's largest producer of niobium and since 2010 the Brazilian government has recommended expanding the use of niobium in industries and fostering its research [9]. In addition, catalysts based on iron and niobium have stood out in several processes, not only due to their natural occurrences and abundances, but also due to their different physical-chemical characteristics that have high applicability in oxidative processes [5]. Thus, in this work, niobium catalysts were developed, modified with iron, for heterogeneous photocatalysis.

## 2. MATERIALS AND METHODS

### Synthesis

The catalysts were prepared from the mixture and solubilization of niobium ammonium oxalate salts ( $\text{NH}_4[\text{NbO}(\text{C}_2\text{O}_4)_2(\text{H}_2\text{O})_2]_n\text{H}_2\text{O}$ ) and nonahydrate ferric nitrate ( $\text{Fe}(\text{NO}_3)_3 \cdot 9\text{H}_2\text{O}$ ). Then, ammonium acetate was added ( $\text{C}_2\text{H}_7\text{NO}_2$ ), in 2 mol molar ratio acetate for every 1 mol iron. The mixture was heated to 60 °C, under constant stirring, until excess moisture was removed. Then, the samples were dried at 120 °C in an oven for 24 h. Finally, the solids were calcined at 400 °C for 2 h and heating rate of 2 °Cmin<sup>-1</sup>. Solids with different concentrations of iron were prepared. The samples were named FeNb0.1, FeNb0.5, FeNb1.0, FeNb1.5, FeNb2.0, according to the ratio (in mol) Nb / Fe0.1, 0.5; 1.0; 1.5; 2.0, respectively.

### Characterization

The solids were characterized by X-ray diffraction (XRD), spectroscopy in the infrared region with Fourier transform infrared spectroscopy (FTIR), point zero charge measurement ( $\text{pH}_{\text{PZC}}$ ) and evaluated in adsorption, Fenton reaction type advanced oxidation and methylene blue heterogeneous photocatalysis.

XRD measurements were performed using a Shimadzu XRD600 diffractometer with a nickel filter. The sample was exposed to CuK  $\alpha$  radiation ( $\lambda = 1.5406 \text{ \AA}$ ), generated at 30 kV and 20 mA. The scan was performed at  $2\theta$  range from 10 ° to 80 °. The samples structural characterization was carried out through crystalline phases identification with automatic search in the crystallographic database Inorganic Crystal Structure Database (ICSD) through Match3 software.

FTIR spectra were generated in the range between 4000 to 400 cm<sup>-1</sup> by means of infrared analyzer with Fourier-PERKIN ELMER transform using Spectrum100-FT-IR model. The solids were analyzed in the form of tablets from the sample diluted in potassium bromide, in the proportion 200:1, using 4 cm<sup>-1</sup> resolution and 32-sweep accumulation.

The point zero charge measurement was carried out at pH range 4 to 11. The solid (0.1 g) was mixed with 7 mL solution whose pH was controlled with the use of hydrochloric acid solutions and

/ or sodium hydroxide ( $0.1 \text{ molL}^{-1}$ ). The mixtures were centrifuged at 100 rpm for 24 h. After centrifugation, the final pH of each suspension was measured with the aid of a pH electrode (TECNOPON brand, resolution 0.01). To measure the  $\text{pH}_{\text{PZC}}$ , the final pH versus initial pH curve was used.

### Catalytic evaluation

Catalytic tests for the removal of methylene blue, by adsorption and oxidation, were carried out according to some authors [10] at  $22 \text{ }^\circ\text{C} \pm 1 \text{ }^\circ\text{C}$  and evaluated by methylene blue absorbance decrease (MB) at  $10 \text{ mg.L}^{-1}$  as a function of the solid exposure time in solution. The evaluation took place with 663nm maximum wavelength, corresponding to the instrumental response sensitivity of UV-vis spectrophotometric (Kasuki model IL-226-BI, with 0.5 cm glass cuvettes) at  $3.5 \text{ mg.L}^{-1}$  of the methylene blue dye concentration, verified by its spectral scanning.

The adsorption tests were carried out in a batch system. 100 mg solid and 50 ml methylene blue dye solution at  $10 \text{ mg.L}^{-1}$  were used. The adsorption was evaluated as a function of time, in which aliquots were removed at different times and centrifuged before measuring their absorbance. The amount of methylene blue adsorbed by the solid was determined from Equation 01.

$$q = \frac{v(C-C_0)}{w} \quad (01)$$

Where  $q$  is the amount of methylene blue adsorbed by mass of catalyst ( $\text{mg.g}^{-1}$ ),  $v$  solution volume (L),  $C$  and  $C_0$  the final and initial concentrations ( $\text{mg.L}^{-1}$ ) respectively and  $w$  is the mass of solid (g). To convert the amount of dye in milligram to percentage, Equation 02 was used.

$$\text{Ads (\%)} = \frac{q}{10} \times 100 \quad (02)$$

Where 10 is the methylene blue concentration used in milligrams per liter ( $10 \text{ mg.L}^{-1}$ ).

The oxidation tests were carried out under the same conditions, but with the addition of 1mL 30% (v / v) hydrogen peroxide to the reactor. Removal was determined using Equation 03.

$$R (\%) = \frac{(A_0-A)}{A_0} \times 100 \quad (03)$$

Where  $R$  is the removal of methylene blue in percentage,  $A_0$  the absorbance at time zero and  $A$  the absorbance at time  $t$ . Methylene blue oxidation by hydrogen peroxide was determined by the difference between the removal processes and the adsorption according to Equation 04.

$$\text{Oxi (\%)} = \text{Rem (\%)} - \text{Ads (\%)} \quad (04)$$

### Effect of the adsorbent amount on adsorption

To find the appropriate amount of mass in the adsorptive system, the influence of the amount of adsorbent on the adsorption was analyzed. The Catalytic Evaluation procedure was carried out using different masses of solids (0.1; 0.2 and 0.3 g).

### Photocatalytic evaluation

In the photocatalysis tests, 250 mL methylene blue solution at  $70 \text{ } \mu\text{molL}^{-1}$  and 0.3 mg catalyst were added to a handcrafted reactor. The reactor outside was in contact with water circulation at  $15 \text{ }^\circ\text{C}$ , in order to maintain its internal temperature at  $30 \text{ }^\circ\text{C}$ . The system was kept under magnetic stirring in the dark for 30 minutes, in order to reach the adsorption equilibrium. After this period, the solution was subjected to U. V. light irradiation by means of mercury steam lamp. The aliquots

were collected at 0.5, 10, 15, 20, 25, 30, 45 and 60, 75 and 90 minutes, centrifuged at 2500 rpm and analyzed using UV-Vis spectrophotometer at 663 nm wavelength.

### 3. RESULTS AND DISCUSSIONS

XRD results (Figure 1) show amorphous halos in the samples with the highest niobium concentration (Fe / Nb 0.5 and 0.1) while the presence of iron favors the crystalline structure. The sample with equimolar Fe/Nb ratio (FeNb1.0) showed the hematite phase and evidence of the formation of a non-stoichiometric iron niobate species ( $\epsilon$ -FeNb<sub>11</sub>O<sub>29</sub>) with orthorhombic phase [6]. The hematite phase is found predominantly in solids with Fe / Nb 1.5 and 2.0 ratios. From the equimolar concentration there is no evidence of secreted niobium oxide. Therefore, there seems to be an isomorphic substitution of iron for niobium in hematite, which may occur due to iron II and niobium IV ionic rays proximity (0.0069 nm and 0.069 nm, respectively). In addition, the reduction and dispersion of niobium oxide particles may have occurred, contributing for the predominant evidence of iron oxide crystalline structure shown by the technique [11].

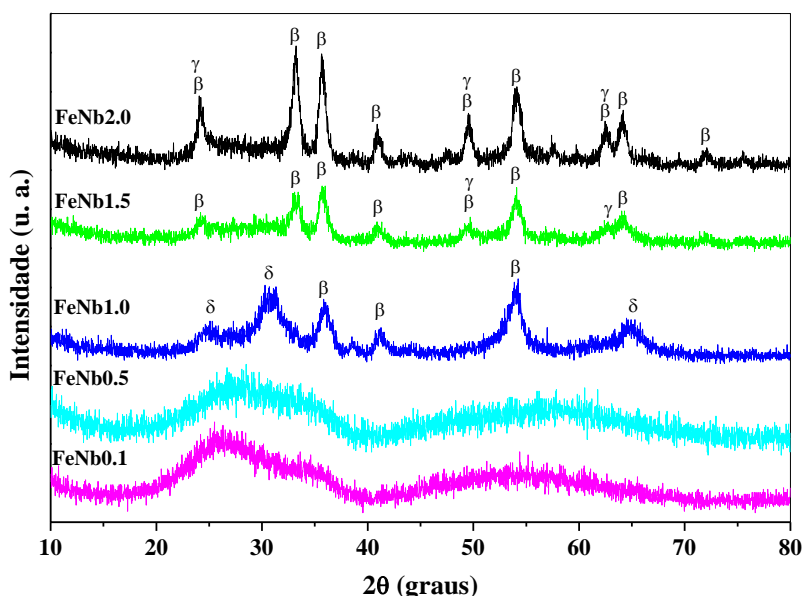


Figure 1. Catalysts diffractograms according to Nb / Fe ratios, with phase identification: hematite ( $\beta$ ), iron tetraoxyniobate III ( $\delta$ ), goethite ( $\gamma$ ).

FTIR spectra (Figure 2), used to evaluate the bonds vibrations present in the materials, showed similar profiles for most samples. In all cases, there is a band centered at approximately 3600  $\text{cm}^{-1}$ , attributed to hydroxyl groups (-OH) stretching of the water present on its surface, with little significant intensity in the FeNb1.0 sample, though, which can be related to the presence of non-stoichiometric iron niobate species in the sample. In addition, there was hydroxyl groups stretching by approximately 3140  $\text{cm}^{-1}$ , commonly observed in solids containing goethite phase (FeOOH) [11].

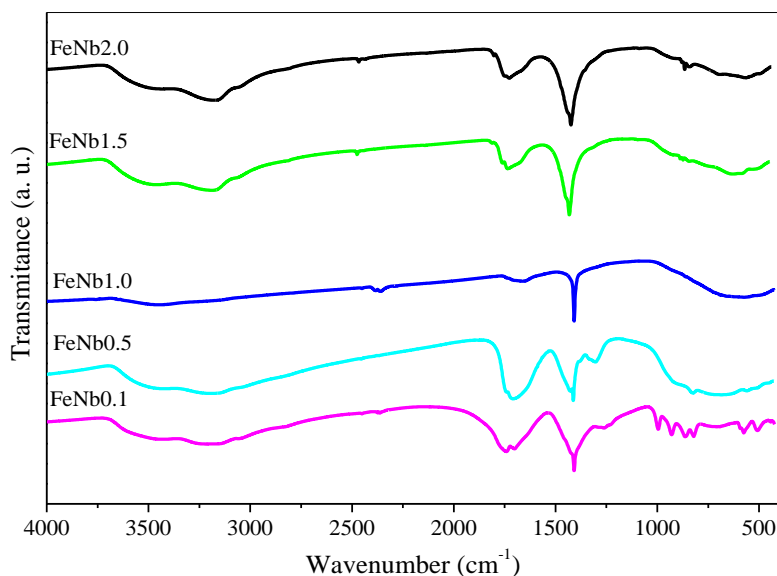


Figure 2. FTIR spectra of calcined samples.

With the exception of FeNb1.0 sample, the materials presented a band centered at  $1700\text{ cm}^{-1}$ , commonly attributed to the  $\text{-C}=\text{O}$  stretch, which may be the result of residual oxalate and acetate species. In all solids, stretches were observed in the region of  $1400\text{ cm}^{-1}$ , with greater intensity for FeNb0.1 and FeNb0.5 samples, though, related to nitrate residues as well as oxalate, demonstrating that the calcination temperature used ( $400\text{ }^{\circ}\text{C}$ ) was not enough for the precursors residues complete elimination (iron nitrate III and ammoniacal niobium oxalate). Finally, bands between  $1000$  and  $400\text{ cm}^{-1}$  point to metal-oxygen bonds with bands at  $840$  and  $680\text{ cm}^{-1}$  regions commonly attributed to the  $\text{-Nb}=\text{O}$  and  $\text{Nb-O-Nb}$  stretch, respectively [12]. The changes observed in bands at lower wave numbers in the samples spectra suggest interactions between the iron and niobium phases present. The Fe / Nb ratio influenced the bands intensity increase at  $1700\text{ cm}^{-1}$  regarding the oxalate ions, due to the higher niobium content, so there was a greater presence of oxalate ions that can be strongly complexed with both metals [13, 14]. Shoulders between  $900\text{-}500\text{ cm}^{-1}$  were identified in the sample with the highest niobium content (FeNb0.5) characteristic of amorphous niobium, phase already identified in the diffractogram for this reason [15, 16].

According to the test to assess the influence of adsorbent amount on adsorption (Figure 3), there was a decrease in the system absorptive capacity with an increase of the adsorbent mass. This behaviour was well evidenced, mainly in the sample with Fe / Nb 2.0 ratio.

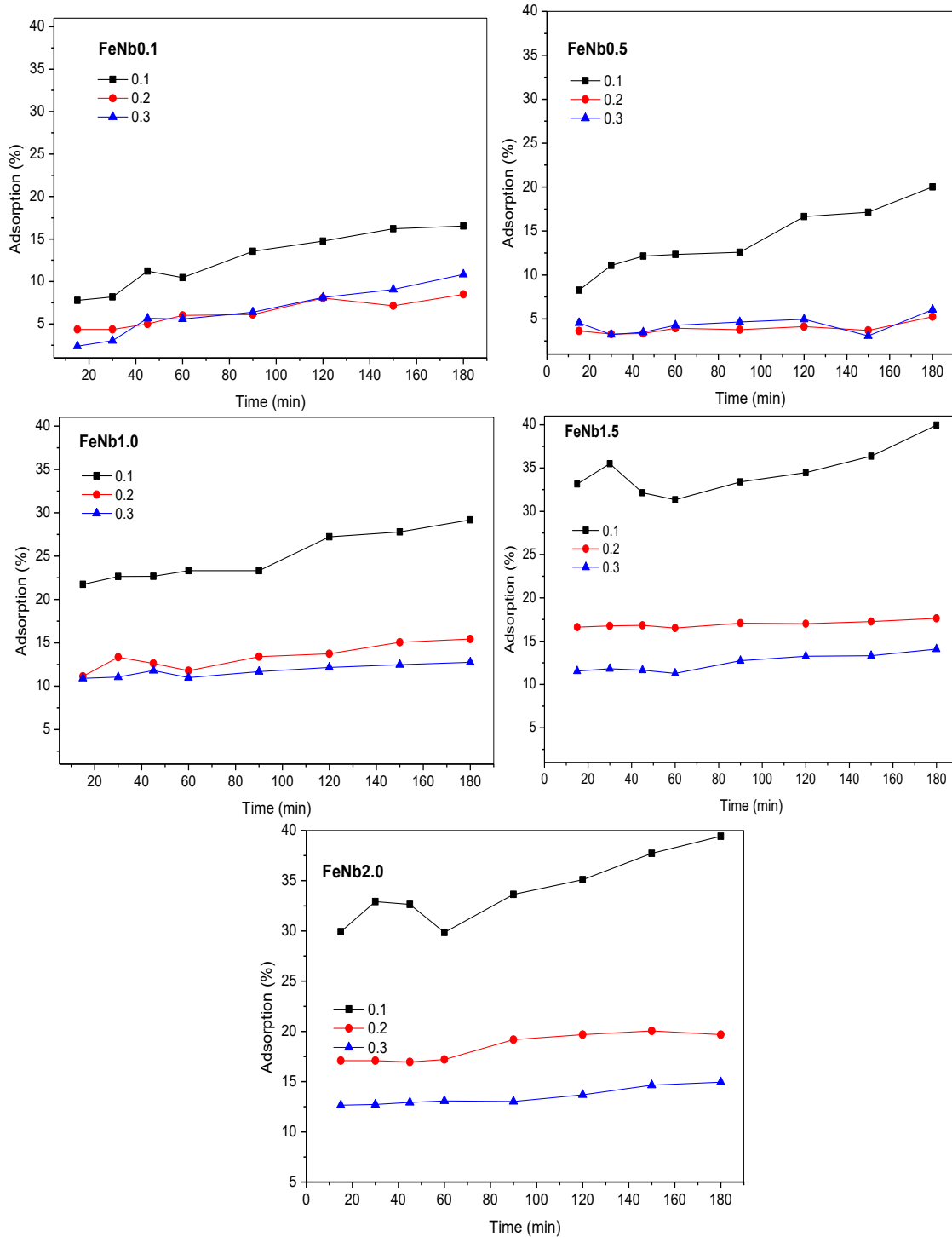


Figure 3. Adsorption curves as a function of time, with different masses.

Dosages above 0.1 g cause materials aggregation, contributing to active sites reduction, significantly decreasing the solids adsorptive capacity. The best performance of materials with 0.1 g mass indicates that the mass decrease favoured a greater dispersion of the solid in solution, and, consequently, a greater charges and pores exposure, responsible for adsorbent-adsorbate interactions. Therefore, the subsequent processes were carried out standardizing 0.1 g mass [17-19].

Figure 4 shows the adsorption curves of methylene blue as a function of time. It was found that the increase in the iron content favoured dye adsorption. Solids with Fe/Nb 2.0 and 1.5 showed

similar behaviour. It can indicate that this concentration range, concerning iron and niobium, is not enough to change the behaviour of solids such as methylene blue adsorbents. However, Fe/Nb 1.0 and Fe/Nb 0.5 ratios showed different behaviour. Therefore, the change in solids behaviour depends on the concentration range.

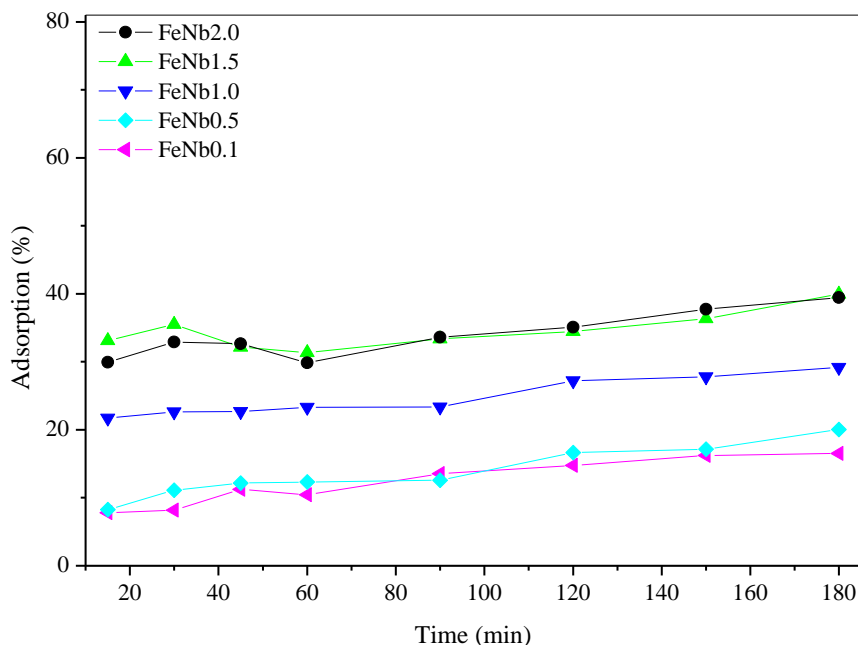


Figure 4. Adsorption curves of solids as function of time.

The increase of niobium content in the materials increases the specific area and reduces the pore diameter; however, it also decreases the materials adsorption capacity, which may justify the lower adsorptive capacity of lower Fe / Nb ratio samples [20, 21].

For weak interactions, as there is no activation energy, this system quickly reaches equilibrium, thus, the interactions present occurred through physisorption. The phenomenon speed can indicate the materials pore size, the presence of small pores favors slow processes of physisorption. Larger pores favor faster and more efficient processes. Thus, the material pore size is reflected in how quickly the system balance is reached, indicating that the material has large pores for this adsorbate [22].

The similarity in solids behavior as adsorbent may be related to the zero point charge, that is, the pH where the charge balance on the material surface is zero (Table 1). Solids with higher iron content (Fe/Nb 1.5 and 2.0) presented  $pH_{PZC}$  values below the pH of the dye solution (pH 5.4). The adsorption of a cationic adsorbate is favored when the solution pH is higher than the material  $pH_{PZC}$ , such as methylene blue dye solution, due to negative charges increase on the solid surface, which may have influenced the better performance of FeNb1.5 and FeNb2.0 samples as adsorbents. The solids with 0.1, 0.5 and 1.0 Fe / Nb ratio showed  $pH_{PZC}$  higher than the solution pH. In this case, the solid surface will acquire a positive charge, causing an electrostatic repulsion and reducing the adsorption capacity of these materials [10, 23]. It can be seen that there was  $pH_{PZC}$  increase along with Nb concentration increase, indicating that niobium decreased the materials acidity, possibly due to residual anionic groups, such as nitrates and mainly oxalates, as already reported for FTIR spectra and with greater intensity for FeNb0.1 and 0.5 ratio samples.

Table 1. Zero point of zero charge values ( $pH_{PZC}$ ), pH of removal process solutions at 180 minutes, bandgap, apparent speed constants ( $k_{ap}$ ) and solids yield coefficient.

Sample	$pH_{PZC}$	pH final	Bandgap (eV)	$k_{ap}$ ( $10^{-3}min^{-1}$ )	$R^2$
FeNb2.0	3.9	4.3	1.8	13.7	0.9989
FeNb1.5	4.3	4.3	1.7	10.2	0.98112
FeNb1.0	6.4	4.2	1.8	19.5	0.9955
FeNb0.5	7.4	4.0	1.8	6.8	0.9787
FeNb0.1	7.2	3.9	-	-	-

The removal curves (Figure 5) show that all solids showed catalytic activity. Fe / Nb2.0 and Fe / Nb1.5 solids showed the best results, with stable curves, reaching equilibrium after 30 min reaction. The other solids, containing iron and niobium, showed constant activity growth during the 180 min reaction.

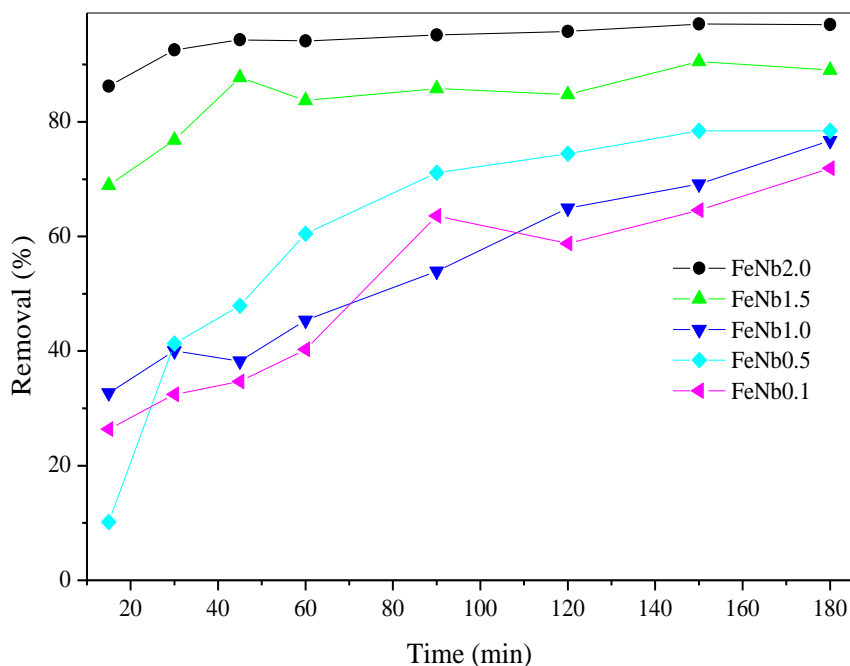


Figure 5. Methylene blue dye removal curve as function of time.

Methylene blue dye removal system picture is shown in Figure 6. In this case, it is possible to observe the liquid mixture turbidity in solids with higher iron concentration due to the formation of iron complexes with water.



Figure 6. Pictures of the methylene blue removal system. From right to left: methylene blue solution, and solutions containing Fe / Nb solids in diets 0.1, 0.5, 1.0, 1.5 and 2.0, respectively.

The dye solution pH was determined at the beginning (pH 5.4) and at the end (Table 1) of the removal process, in which a decrease in pH was observed in all systems, resulting from iron hydroxides formation, characterized by dark green color (Figure 7). For iron hydroxides formation,  $H^+$  ions are released in solution, which may be related to the decrease in the catalytic system pH (Table 1). After a few minutes of reaction the solution showed brown color; it is possible to observe the liquid mixture turbidity in solids with higher iron concentration due to the formation of iron complexes with water, from particles of hydrated iron oxides ( $Fe_2O_3 \cdot H_2O_n$ ) [24, 25].

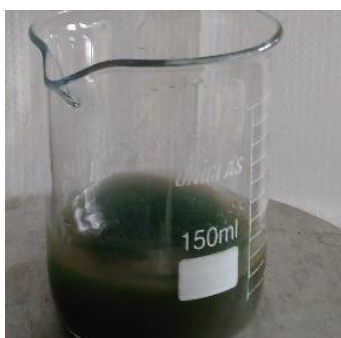
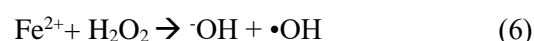


Figure 7. Picture of the removal system at the beginning of the reaction.

Figure 8 shows the oxidation curves attributed to the solids catalytic behavior. Fe / Nb2 sample showed approximately 60% oxidation throughout the reaction time, being, therefore, the most active and stable catalyst, demonstrating that the increase in iron concentration favored the material catalytic activity. The other samples showed an increase in oxidation capacity over time, especially the Fe/Nb0.1 ratio sample. The catalytic results demonstrate that the combined materials of iron oxides and niobium have high potential in organic compounds oxidation reactions, mainly materials with small niobium concentration. Other works have also reported the efficiency of these materials and the importance of niobium for their catalytic activity [26].

$Fe^{3+}$  ions (Eq. 5) can generate intermediate radicals receiving an electron from  $H_2O_2$  and through electron donation,  $Fe^{2+}$  ions producing  $\bullet OH$  radicals (Eq. 6). Both  $\bullet OH$  and intermediate radicals ( $HO_2\bullet$ ) are responsible for dye oxidation. However,  $\bullet OH$  radicals have greater oxidative potential, so they are more effective in the system [27, 28].



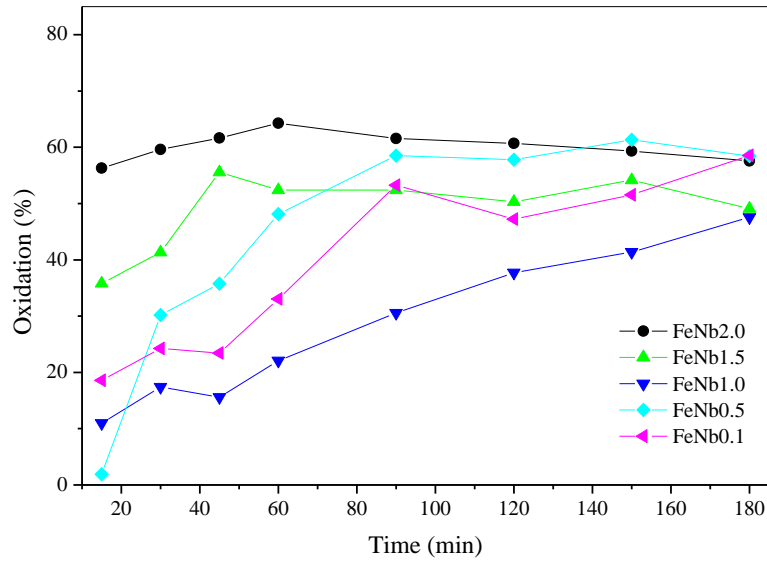


Figure 8. Catalytic curves of methylene blue dye oxidation.

Materials bandgap values (Table 1) suggest that all solids have semiconductors electronic properties [29-31]. The solids showed practically the same result (1.8 eV) and sample FeNb1.5 favored a little more the reduction of the prohibited band (1.7 eV), demonstrating that this ratio can potentiate photocatalytic reactions even more [32]. This factor generates advantages in the use of mixed oxides based on iron and niobium, since pure niobium oxide absorbs light in the ultraviolet region (bandgap from 3.1 to 4.0 eV) and mixed oxides have spectral photosensitivity in the visible range, being possible to use sunlight as energy source [30, 33, 34].

Photocatalytic test results for FeNb samples are shown in Figure 9 and in Table 1. It is observed that the sample with twice the niobium content (FeNb0.5) showed the worst performance leading to a 44% methylene blue discoloration after 90-minute testing. On the other hand, samples with higher iron concentration led to an improvement in photocatalytic performance reaching 81% for FeNb1.0 sample and 70% for FeNb 2.0 system, after 90 minutes. The best photocatalytic performance of FeNb1.0 sample may be associated with the presence of iron niobate phase ( $\epsilon$ -FeNb<sub>11</sub>O<sub>29</sub>) once this phase can improve the optical absorption in U.V and visible light region significantly [6, 35].

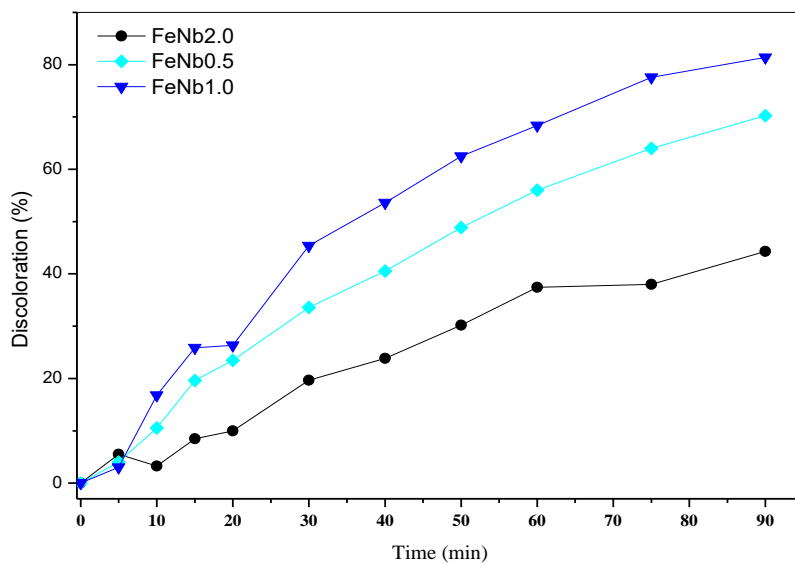


Figure 9. Discoloration of methylene blue solution in photocatalysis.

For a better comparison of different solids effect regarding process kinetics, the data were adjusted to Langmuir-Hinshelwood model (Eq. 7). According to the literature, organic pollutants oxidation in aqueous suspension follows the aforementioned model [25].

$$-\frac{dC}{dt} = k_r \frac{K_a C}{1 + K_a C} \quad (7)$$

Considering a very small C value,  $K_a C$  product can be neglected in the denominator. Using the pseudo first order model, and being:  $C = C_0$  and  $t = 0$ , Equation 8 is obtained.

$$-\ln\left(\frac{C}{C_0}\right) = kt \quad (8)$$

Since k is the apparent constant of pseudo first order that can be determined by plotting  $\ln(C/C_0)$  as function of time. In general, the fit of data to the model was satisfactory, considering R values. k values are shown in Table 1.

The comparison between the apparent velocity constants values further evidence the materials different behaviour towards the process kinetics, with the k value obtained by using Fe/Nb 1 sample being higher than the others, followed by Fe/Nb 0.5 sample. This effect cannot be associated with the bandgap, once there is no significant difference between them.

#### 4. CONCLUSIONS

In this work, solids based on iron oxide and niobium oxide were developed in different Fe / Nb ratios, using complexing precursor salts and heat treatment at 400 °C, characterized and evaluated in the Fenton reaction and photocatalysis. It was observed that only solids with Fe/Nb ratio equal to or greater than the equimolar one showed crystalline structure at X-rays. Fe/Nb 2 ratio solid showed predominantly hematite phase and goethite evidence. Fe/Nb2 ratio solid also showed the best result as a catalyst, but there was no linear relationship between the Fe/Nb ratio and the catalytic performance of the solids.

On the other hand, the increase in niobium concentration increased the zero point charge values and decreased the reaction system final pH. Fe/Nb2 ratio solid also showed the best performance as an adsorbent and in oxidation reaction, followed by the Fe/Nb1.5 ratio one. The solids showed practically the same result (1.8 eV), It is observed that the presence of iron niobate (FeNb1.0) favours the photocatalytic system.

#### 5. ACKNOWLEDGMENT

The authors would like to thank FAPESB and PRPGI-IFBA for funding through scientific initiation grants.

#### 6. REFERENCES

1. Hodges BC, Cates EL, Kim JH. Challenges and prospects of advanced oxidation water treatment processes using catalytic nanomaterials. *Nature Nanotechnol.* 2018;13(8):642-650, doi: 10.1038/s41565-018-0216-x
2. Lee SY, Park SJ. TiO<sub>2</sub> photocatalyst for water treatment applications. *J Ind Eng Chem.* 2013;19(6):1761–1769, doi: 10.1016/j.jiec.2013.07.012
3. Crini G, Lichtfouse E. Advantages and disadvantages of techniques used for wastewater treatment. *Environmental Chem Lett.* 2019;17:145-155, doi: 10.1007/s10311-018-0785-9
4. Britto JM, Rangel MDC. Processos avançados de oxidação de compostos fenólicos em efluentes industriais. *Quim Nova.* 2008;31(1):114-122, doi: 10.1590/S0100-40422008000100023

5. Lopes OF, Mendonça VR de, Silva FBF, Paris EC, Ribeiro C. Niobium oxides: an overview of the synthesis of Nb<sub>2</sub>O<sub>5</sub> and its application in heterogeneous photocatalysis. *Quim Nova*. 2015;38(1):106-117, doi: 10.5935/0100-4042.20140280
6. Cho I-S, Lee S, Noh JH, Choi GK, Jung HS, Kim DW, et al. Visible-light-induced photocatalytic activity in FeNbO<sub>4</sub> nanoparticles. *J Phys Chem C*. 2008;112(47):18393-18398, doi: 10.1021/jp807006g
7. Gonçalves M, Oliveira LCA, Guerreiro MC. Nióbia magnética como adsorvente de contaminantes orgânicos em meio aquoso: efeito da temperatura e do pH. *Quim Nova*. 2008;31(3):518-522, doi: 10.1590/S0100-40422008000300010
8. Prado NT, Oliveira LCA. Nanostructured niobium oxide synthesized by a new route using hydrothermal treatment: High efficiency in oxidation reactions. *Appl Catalysis B: Environm*. 2017;205:481-488, doi: 10.1016/j.apcatb.2016.12.067
9. Bruziquesi C, Balena J, Pereira M, Silva A, Oliveira L. Nióbio: um elemento químico estratégico para o Brasil. *Quim Nova*. 2019;4(10):1184-1188, doi: 10.21577/0100-4042.20170442
10. Huang G, Wang D, Ma S, Chen J, Jiang L, Wang P. A new, low-cost adsorbent: Preparation, characterization, and adsorption behavior of Pb(II) and Cu(II). *J Colloid Interface Sci*. 2015;445:294-302, doi: 10.1016/j.jcis.2014.12.099.
11. NIST: National Institute of Standards and Technology [Internet]. National Institute of Standards and Technology - Secretary of Commerce on behalf of the United States of America. 2018 [cited 2020 Jul]. Available from: <https://webbook.nist.gov/chemistry/>
12. Nagarajan S, Raman V, Rajendran N. Síntese e caracterização eletroquímica de óxido de nióbio poroso revestido com 316L SS para aplicações ortopédicas. *Mat Chem Phys*. 2010;119(3):363-366, doi: 10.1016/j.matchemphys.2009.10.033
13. Pinto MB, Soares AL, Mella Orellana A, Duarte HA, De Abreu HA. Structural, electronic, and thermodynamic properties of the T and B phases of niobia: first-principle calculations. *J Phys Chem A*. 2017;121(12):2399-2409, doi: 10.1021/acs.jpca.6b11383
14. Huang H, He D, Tang Y, Guo Y, Li P, Qv W, et al. Adsorption of hexavalent chromium from an aqueous phase by hydroxypropyl methylcellulose modified with diethylenetriamine. *J Chem Eng Data*. 2019 Jan 10;64(1):98-106, doi: 10.1021/acs.jced.8b00607
15. Ristić M, Popović S, Musić S. Sol-gel synthesis and characterization of Nb<sub>2</sub>O<sub>5</sub> powders. *Mater Lett*. 2004;58(21):2658-2663, doi: 10.1016/j.matlet.2004.03.041
16. Maschio LJ, Pereira PHF, da Silva MLCP. Preparation and characterization of cellulose/hydrous niobium oxide hybrid. *Carbohydrate Polymers*. 2012;89(3):992-996, doi: 10.1016/j.carbpol.2012.04.043
17. Wang X, Wang Y, Hou H, Wang J, Hao C. Ultrasonic method to synthesize glucan-g-poly(acrylic acid)/sodium lignosulfonate hydrogels and studies of their adsorption of Cu<sup>2+</sup> from aqueous solution. *ACS Sustain Chem Eng*. 2017;5(8):6438-6446, doi: 10.1021/acssuschemeng.7b00332
18. Rahimi Bourestan N, Nematollahzadeh A, Parchehbaf Jadid A, Basharnavaz H. Chromium removal from water using granular ferric hydroxide adsorbents: An in-depth adsorption investigation and the optimization. *Chem Phys Lett*. 2020;748:137395, doi: 10.1016/j.cplett.2020.137395
19. Sharma P, Singh AK, Shahi VK. Selective adsorption of Pb(II) from aqueous medium by cross-linked chitosan-functionalized graphene oxide adsorbent. *ACS Sustain Chem Eng*. 2019 Jan;7(1):1427-1436, doi: 10.1021/acssuschemeng.8b05138
20. Nowak I, Jaroniec M. Three-dimensional cubic mesoporous molecular sieves of FDU-1 containing niobium: Dependence of niobium source on structural properties. *Langmuir*. 2005 Jan;21(2):755-760, doi: 10.1021/la048157i
21. Carniti P, Gervasini A, Marzo M. Dispersed NbO<sub>x</sub> catalytic phases in silica matrixes: influence of niobium concentration and preparative route. *J Phys Chem C*. 2008 Sep;112(36):14064-14074, doi: 10.1021/jp803140x
22. Karimi S, Tavakkoli Yarak M, Karri RR. A comprehensive review of the adsorption mechanisms and factors influencing the adsorption process from the perspective of bioethanol dehydration. *Renew Sustain Energy Rev*. 2019 Jun;107:535-553, doi: 10.1016/j.rser.2019.03.025
23. Cazetta AL, Pezoti O, Bedin KC, Silva TL, Paesano Junior A, Asefa T, et al. Magnetic activated carbon derived from biomass waste by concurrent synthesis: Efficient adsorbent for toxic dyes. *ACS Sustain Chem Eng*. 2016 Mar;4(3):1058-1068, doi: 10.1021/acssuschemeng.5b01141
24. de Ávila SG, Matos JR. Compostos coloridos do ferro: uma proposta de experimentação utilizando materiais de baixo custo. *Educ Química*. 2017;28(4):254-261, doi:10.1016/j.eq.2017.04.001
25. Cornell RM, Schwertmann U. The iron oxides. Darmstadt (Germany): Wiley-VCH Verlag GmbH & Co. KGaA, Weinheim; 2003, doi:10.1002/3527602097
26. Rezende CC, Neto JL, Silva AC, Lima VM, Pereira MC, Oliveira LCA. Synthesis and characterization of iron/niobium composites: Catalyst for dye wastewater treatments. *Catal Commun*. 2012;26:209-213, doi: 10.1016/j.catcom.2012.06.006

27. Fang L, Liu Z, Zhou C, Guo Y, Feng Y, Yang M. Degradation mechanism of methylene blue by H<sub>2</sub>O<sub>2</sub> and synthesized carbon nanodots/graphitic carbon nitride/Fe(II) composite. *J Phys Chem C*. 2019 Nov;123(44):26921-26931, doi: 10.1021/acs.jpcc.9b06774
28. Yang M, Zhang X, Grosjean A, Soroka I, Jonsson M. Kinetics and mechanism of the reaction between H<sub>2</sub> O<sub>2</sub> and tungsten powder in water. *J Phys Chem C*. 2015 Oct;119(39):22560-22569, doi: 10.1021/acs.jpcc.5b07012
29. Oliveira HS. Óxidos de ferro dotados com vanádio ou nióbio como catalisadores em reações de oxidação [master's dissertation]. Belo Horizonte (MG): Universidade Federal de Minas Gerais; 2013. 77 p. Available from: <https://repositorio.ufmg.br/handle/1843/SFSA-9ATR8X>
30. Aroutiounian VM, Arakelyan VM, Shahnazaryan GE, Stepanyan GM, Khachatryan EA, Wang H, et al. Photoelectrochemistry of semiconductor electrodes made of solid solutions in the system Fe<sub>2</sub>O<sub>3</sub>-Nb<sub>2</sub>O<sub>5</sub>. *Sol Energy*. 2006;80(9):1098-1111, doi: 10.1016/j.solener.2005.10.005
31. Geng L, Jian W, Jing P, Zhang W, Yan W, Bai F-Q, Liu G. Crystal phase effect of iron oxides on the aerobic oxidative coupling of alcohols and amines under mild conditions: A combined experimental and theoretical study. *J Catalysis*. 2019;377:145-152, doi: 10.1016/j.jcat.2019.06.018
32. Silva AC, Bruziquesi CGO, Almeida MR, Rodriguez M, Oliveira HS, Machado ART, et al. Converting Fe-rich magnetic wastes into active photocatalysts for environmental remediation processes. *J Photochem Photobiol A Chem*. 2017;335:259-267, doi: 10.1016/j.jphotochem.2016.11.025
33. Baccaro A, Gutz I. Fotoeletrocatalise em semicondutores: dos princípios básicos até sua conformação à nanoescala. *Quim Nova*. 2018;41(3):326-339, doi: 10.21577/0100-4042.20170174;
34. Brasileiro ILO, Madeira VS, de Souza CP, Lopes-Moriyama AL, Ramalho MLRA, Araújo AAD. Development of  $\alpha$ -Fe<sub>2</sub>O<sub>3</sub>/Nb<sub>2</sub>O<sub>5</sub> photocatalysts by a Pechini sol-gel route: Structural, morphological and optical influence. *Mater Res Express*. 2018;6(1):015043, doi: 10.1088/2053-1591/aae8cb
35. Miyake H, Kozuka H. Photoelectrochemical properties of Fe<sub>2</sub>O<sub>3</sub>-Nb<sub>2</sub>O<sub>5</sub> films prepared by sol-gel method. *J Phys Chem B*. 2005;109(38):17951-17956, doi: 10.1021/jp058051b